



## Photodecolorization of methyl orange over $\alpha$ -Fe<sub>2</sub>O<sub>3</sub>-supported HY catalysts: The effects of catalyst preparation and dealumination

Nur Farhana Jaafar<sup>a</sup>, Aishah Abdul Jalil<sup>b,\*</sup>, Sugeng Triwahyono<sup>a</sup>, Muhd Nazlan Muhd Muhid<sup>c</sup>, Norzahir Sapawe<sup>b</sup>, Mohammad Azrul Hisham Satar<sup>b</sup>, Hanak Asaari<sup>b</sup>

<sup>a</sup> Ibnu Sina Institute for Fundamental Science Studies, Faculty of Science, Universiti Teknologi Malaysia, 81310 UTM Skudai, Johor, Malaysia

<sup>b</sup> Institute of Hydrogen Economy, Faculty of Chemical Engineering, Universiti Teknologi Malaysia, 81310 UTM Skudai, Johor, Malaysia

<sup>c</sup> Department of Chemistry, Faculty of Science, Universiti Teknologi Malaysia, 81310 UTM Skudai, Johor, Malaysia

### ARTICLE INFO

#### Article history:

Received 19 October 2011

Received in revised form 26 February 2012

Accepted 27 February 2012

#### Keywords:

$\alpha$ -Fe<sub>2</sub>O<sub>3</sub>/HY catalyst

Electrochemical

Dealumination

Photodecolorization

Methyl orange

### ABSTRACT

An  $\alpha$ -Fe<sub>2</sub>O<sub>3</sub>-supported HY zeolite ( $\alpha$ -Fe<sub>2</sub>O<sub>3</sub>/HY) was prepared by introducing nanosized  $\alpha$ -Fe<sub>2</sub>O<sub>3</sub> into an HY zeolite support through in situ ( $\alpha$ -Fe<sub>2</sub>O<sub>3</sub>/HY<sub>IS</sub>) and ion-exchange ( $\alpha$ -Fe<sub>2</sub>O<sub>3</sub>/HY<sub>IE</sub>) methods. The effect of the preparation methods on the physicochemical properties of the catalyst were studied via XRD, FESEM-EDX, TEM, UV-vis DRS, FTIR, XPS, <sup>29</sup>Si and <sup>27</sup>Al MAS NMR, ESR and BET surface area analysis. In this study, dealumination was accomplished by using a facile electrolysis system without any strong acids, reactive compounds and/or hydrothermal treatment. Dealumination accompanied by ion exchange of Al with Fe<sup>3+</sup> ions in the HY zeolite framework resulted in the formation of an active species that had a higher photoactivity towards the decolorization of methyl orange (MO). A 5 wt%  $\alpha$ -Fe<sub>2</sub>O<sub>3</sub>/HY<sub>IS</sub> was found to produce an 80% photodecolorization of 30 mg L<sup>-1</sup> of MO at pH 2 with 0.375 g L<sup>-1</sup> catalyst, while 5 wt%  $\alpha$ -Fe<sub>2</sub>O<sub>3</sub>/HY<sub>IE</sub> only produced 23% photodecolorization under similar conditions (2 h reaction time). This study showed that the kinetics follow a pseudo-first order Langmuir–Hinshelwood model with an activation energy (*E<sub>a</sub>*) calculated for both 5 wt%  $\alpha$ -Fe<sub>2</sub>O<sub>3</sub>/HY<sub>IS</sub> and 5 wt%  $\alpha$ -Fe<sub>2</sub>O<sub>3</sub>/HY<sub>IE</sub> to be 45.8 kJ mol<sup>-1</sup> and 70.2 kJ mol<sup>-1</sup>, respectively. Measurements of the mineralization of MO by COD, BOD<sub>5</sub> and TOC analysis were 27.0%, 69.6% and 16.9%, respectively, after 2 h of contact time. The Fe dissolution from the catalyst showed insignificant leaching of Fe (<1%) when subjected to AAS. A reusability study demonstrated that  $\alpha$ -Fe<sub>2</sub>O<sub>3</sub>/HY<sub>IS</sub> could be a promising photocatalyst for the degradation of various dyes in wastewater.

© 2012 Elsevier B.V. All rights reserved.

### 1. Introduction

Many industries, such as the textile, paint and plastics industries, currently use synthetic dyes in their production processes. Synthetic dyes are widely used in the textile industries because of their stable chemical structures can withstand the washing process to meet various coloring requirements [1]. Every year, 800,000 tons of dyes are produced worldwide, and approximately half of them are azo dyes [2]. Azo dyes are characterized by the presence of N=N groups; methyl orange is a common water-soluble azo dye [3]. These aromatic amines cannot easily be degraded and are suspected to be carcinogenic and mutagenic to humans, in addition to reducing light penetration in bodies of water, which is harmful to aquatic life [4]. Therefore, a variety of conventional treatments are widely used, such as coagulation [5], flocculation [6], adsorption on activated carbon [7] and membrane filtration [8]. However, these treatment technologies are less effective and still need to be

developed, especially for the treatment of secondary wastes, which may sometimes be more toxic than the first degraded products.

Advanced oxidation processes (AOPs), especially photocatalysis, have become a popular method for wastewater treatment because they convert contaminants, to a large extent, into stable, inorganic compounds, such as carbon dioxide and water. The abundance of hydroxyl radicals generated by the AOPs plays an important role in oxidizing the organic species present in the wastewater into harmless species [9]. Heterogeneous photocatalysis by semiconductor materials, such as TiO<sub>2</sub>, ZnO, Fe<sub>2</sub>O<sub>3</sub>, CdS, GaP and ZnS, have been widely used in photocatalytic degradation [10]. Among them, TiO<sub>2</sub> has been widely researched for photocatalytic applications, but its wide band gap (~3.2 eV) limits its practical application because it can only be excited by ultraviolet light, but not visible light.

The surface area, size distribution and band gap become important properties to be considered in order to increase the photocatalytic activity [11]. Hematite ( $\alpha$ -Fe<sub>2</sub>O<sub>3</sub>), with a band gap of 2.2 eV, is a good candidate as a photocatalyst because it can absorb visible light [12]. However, it produces high concentrations of iron ions in the bulk in use, which requires secondary treatment. This limitation can be overcome by finding a suitable support for

\* Corresponding author. Tel.: +60 7 5535581; fax: +60 7 5536165.

E-mail addresses: [aishah@cheme.utm.my](mailto:aishah@cheme.utm.my), [aishah.aj@gmail.com](mailto:aishah.aj@gmail.com) (A. Abdul Jalil).

$\alpha$ -Fe<sub>2</sub>O<sub>3</sub> to modify the catalyst surface and reduce iron dissolution [13]. Support materials, such as zeolites and clay, have a low polar surface and a large surface area, as well as a high adsorption capacity for non-polar and organic pollutants. Most of the previous studies which involved the degradation of dyes using iron supported zeolite showed that iron was well dispersed on the support materials and resulted in a high catalytic activity without any Fe ion leaching [14–20]. Chen and Zhu degraded acid light yellow G using Fe-pillared bentonite and found that the catalyst possessed long-term stability and strong surface activity [21].

Previously, we reported a new electrochemical method for the synthesis of zinc nanoparticles with higher reactivity and its successful use in the synthesis of anti-inflammatory agent precursors [22]. The modification of nanosized zinc metal supported on a HZSM5 zeolite seemed to facilitate the generation of protonic acid sites for the enhancement of *n*-alkane isomerization [23]. Nanoparticles of zinc prepared by simple electrochemical method possess a higher surface area and seem to be advantageous for both of the reactions. Therefore, as an extension of the previous study, we intend to synthesize nanoparticles of  $\alpha$ -Fe<sub>2</sub>O<sub>3</sub> supported on HY zeolites by the electrochemical method and study the photoactivity of this type of nanomaterial in the decolorization of methyl orange. The physicochemical properties of the catalyst were studied in detail via XRD, TEM, FESEM-EDX, UV–vis DRS, FTIR, XPS, and <sup>29</sup>Si and <sup>27</sup>Al MAS NMR, ESR and BET surface area analysis. Kinetic studies, the proposed mechanism of photodecolorization, and the reusability and biodegradability of the catalysts are also discussed.

## 2. Experimental

### 2.1. Reagents and materials

Methyl orange (MO), perchloric acid, *N,N*-dimethylformamide (DMF) and hydrochloric acid were purchased from MERCK, Malaysia and acetone was purchased from HmbG Chemical. Naphthalene and tetraethylammonium bromide solution were purchased from Fluka Chemical and methanol was purchased from RPE Reagent Pure Erba. Zeolite Y with a silica/alumina ratio of 80 was purchased from Zeolyst International. Iron and platinum plates of greater than 99% purity were used as electrodes and were obtained from Nilaco, Japan. Tetraethylammonium perchlorate (TEAP), which was used as a supporting electrolyte in electrolysis, was prepared in accordance with the procedure reported in the literature [24].

### 2.2. Preparation of the catalyst

In this study, two types of preparation methods, *in situ* (IS) and *ion-exchange* (IE) were carried out. The experimental procedures of both techniques were similar to those reported in the literature [24]. For the *in situ* preparation technique, a 10 mL of DMF solution was added to a one-compartment cell fitted with a platinum plate cathode (2 cm × 2 cm) and an iron plate anode (2 cm × 2 cm) containing TEAP, naphthalene and HY zeolite. Naphthalene was used as a mediator in the system to produce radical anions, which then reduced the iron cations to give much smaller iron nanoparticles [22]. Then, the electrolysis was conducted at a constant current of 60 mA/cm<sup>2</sup> and 0 °C under a N<sub>2</sub> atmosphere under continuous stirring. The required iron loading on the HY support was calculated based on Faraday's law of electrolysis, as shown in the following equation,

$$n = \left( \frac{It}{F} \right) \left( \frac{1}{z} \right) \quad (1)$$

where *n* is the number of moles of Fe, *I* is constant current of electrolysis (A), *t* is the total time the constant current was applied

(s), *F* is the Faraday constant (96,487 C mol<sup>-1</sup>), and *z* is the valency number of ions of the substance (electron transferred per ion). The number of moles of Fe required was calculated based on the total time *t* of the electrolysis. For example, 1137 s is the time required to produce 5 wt% of Fe in 1.5 g HY. After electrolysis, the mixture was impregnated at 80 °C in an oil bath before being dried overnight at 100 °C and calcined for 3 h at 550 °C to give a brown-colored  $\alpha$ -Fe<sub>2</sub>O<sub>3</sub>/HY<sub>IS</sub> catalyst.

The experimental procedure for the *ion-exchange* method is similar to the above except that the HY was added to the mixture after electrolysis. The mixture was then impregnated, oven dried and calcined as above, and finally, a brown-colored  $\alpha$ -Fe<sub>2</sub>O<sub>3</sub>/HY<sub>IE</sub> catalyst was obtained, which was ready for characterization.

### 2.3. Catalyst characterization

X-ray diffraction (XRD) was carried out using a Bruker Advance D8 X-ray powder diffractometer (Cu K $\alpha$  radiation,  $\lambda = 1.5418 \text{ \AA}$ ). Transmission electron microscopy (TEM) was carried out using a JEOL JEM-2100F. The catalysts were ultrasonically dispersed in acetone and deposited on amorphous, holey carbon membranes. Field-emission scanning electron microscopy was conducted using energy dispersion X-ray spectroscopy (FESEM-EDX, JEOL JSM-6701F) to determine the elemental composition of the samples. UV–vis diffuse reflectance spectra (UV–vis DRS) were recorded in air at room temperature over a range of wavelengths from 400 to 850 nm using a Perkin Elmer Lambda 900 UV/VIS/NIR spectrometer with an integrating sphere. FTIR spectroscopy (Perkin Elmer Spectrum GX FTIR Spectrometer) was performed to identify the chemical functional groups present in the catalysts. IR absorbance data were obtained over a range of wavenumbers from 400 to 4000 cm<sup>-1</sup>. The chemical oxidation of the  $\alpha$ -Fe<sub>2</sub>O<sub>3</sub>/HY<sub>IS</sub> catalyst was determined using X-ray photoelectron spectroscopy (XPS) conducted on a Kratos Ultra spectrometer equipped with an Mg K $\alpha$  radiation source (10 mA, 15 kV) over a range of binding energies from 0 to 800 eV. A powdered sample was pressed into a small Inox cylinder and analyzed inside an analysis chamber at  $1 \times 10^{-10}$  Pa. To correct for the energy shift due to surface charging of the samples, the binding energy of the C (1s) peak at  $284.5 \pm 0.1$  eV was set as an internal standard. Nuclear magnetic resonance measurements were carried out using <sup>29</sup>Si and <sup>27</sup>Al Magic Angle Spinning Nuclear Magnetic Resonance (MAS NMR) Spectroscopy, which was performed at room temperature on a Bruker Solid NMR (JEOL 400 MHz) spectrometer using tetramethylsilane (TMS) as an external reference. Chemical species with unpaired electrons were studied by bombarding the sample with UV-light (from a 500 W high-pressure Hg lamp) coupled with Electron Spinning Resonance (ESR) Spectroscopy (JEOL JES-FA 100) for several minutes at room temperature. Nitrogen adsorption–desorption isotherms were used to determine the textural properties at liquid nitrogen temperatures using a Micromeritics ASAP 2010 instrument. The Brunnauer–Emmett–Teller (BET) and Barrett–Joyner–Halender (BJH) methods were used to calculate surface area and pore distribution, respectively. Prior to measurement, all of the samples were degassed at 110 °C and 0.1 Pa.

### 2.4. Photodecolorization of methyl orange

The photoactivity of the catalysts was tested for the decolorization of MO. The photocatalytic experiments were performed in a batches consisting of 250 ml Pyrex conical flasks placed on a magnetic stirrer to uniformly disperse the catalyst into solution. A fluorescent lamp (20 W) light source was mounted 10 cm above the solution. The entire was placed inside a chamber covered with aluminum foil to prevent the passage of other lights into the reactor.

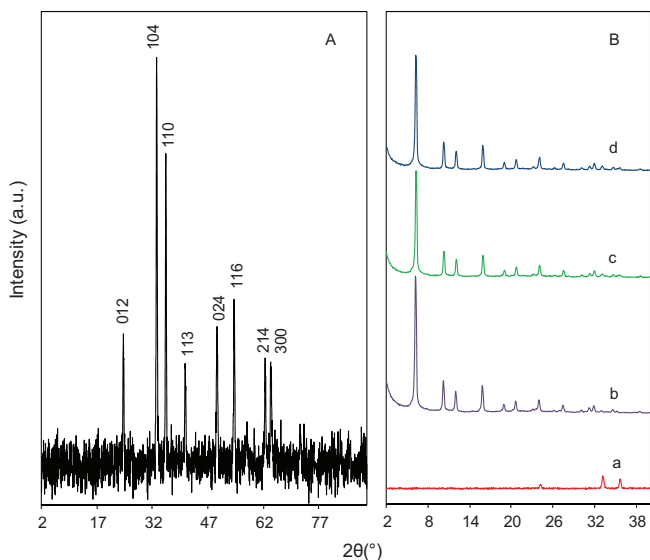


**Fig. 1.** XRD diffractograms of (A)  $\alpha$ -Fe<sub>2</sub>O<sub>3</sub> prepared by electrochemical method; and (B) (a)  $\alpha$ -Fe<sub>2</sub>O<sub>3</sub>, (b) HY, (c)  $\alpha$ -Fe<sub>2</sub>O<sub>3</sub>/HY<sub>IS</sub>, and (d)  $\alpha$ -Fe<sub>2</sub>O<sub>3</sub>/HY<sub>IE</sub>.

For photoactivity evaluation, 0.375 gL<sup>-1</sup> of catalyst was added to the MO solution with a desired concentration (200 mL) and stirred for 2 h in the dark to achieve adsorption–desorption equilibrium. The initial pH of the solution was 2 and the reaction was carried out at 30 °C. Then, the reaction was carried out for another 2 h under light irradiation under continuous stirring. The concentration of MO dye in the solution prior to irradiation was used as the initial value for the MO decolorization measurements.

During the reaction, aliquots of 2 ml were taken out at intervals of 15 min and centrifuged in a Hettich Zentrifugen Micro 120 at 75,000 rpm for 10 min before being analyzed by UV–vis spectrophotometry (Thermo Scientific Genesys 10uv Scanning) for the residual concentration of MO. Each set of experiments was performed three times. The adsorption band of MO was taken at 506 nm and the decolorization percentage was calculated using the following equation:

$$\text{Decolorization}(\%) = \frac{C_0 - C_t}{C_0} \times 100 \quad (2)$$

where  $C_0$  and  $C_t$  are the initial concentration of MO and the concentration at time  $t$ , respectively.

The elemental analyses of Fe in solution were determined by atomic absorption spectroscopy (AAS) using a Perkin-Elmer model A Analyst 400 Atomic Absorption Spectrophotometer. BOD was measured using a YSI model 33 in which BOD bottles were incubated at 20 °C for 5 days; the difference in the dissolved oxygen was used to calculate BOD<sub>5</sub>. A HACH DR4000 spectrometer was used for COD measurements. In addition, the total organic carbon (TOC) removal was determined using a TOC Shimadzu Vcph spectrophotometer for each experiment before and after a reaction time of 2 h for the evaluation of the mineralization of MO dye. TOC was calculated as the difference between the total carbon (TC) and inorganic (IC) in the liquid sample.

### 3. Results and discussion

#### 3.1. Physicochemical properties of the prepared catalyst

The XRD patterns of HY and the prepared  $\alpha$ -Fe<sub>2</sub>O<sub>3</sub>,  $\alpha$ -Fe<sub>2</sub>O<sub>3</sub>/HY<sub>IS</sub> and  $\alpha$ -Fe<sub>2</sub>O<sub>3</sub>/HY<sub>IE</sub> are shown in Fig. 1. Several peaks were observed for  $\alpha$ -Fe<sub>2</sub>O<sub>3</sub> in Fig. 1A at  $2\theta = 24.1^\circ, 33.1^\circ, 35.6^\circ, 40.75^\circ, 49.3^\circ, 54.05^\circ, 62.4^\circ, 62.55^\circ$ , and these peaks are similar to the typical peaks

**Table 1**

The  $d$ -value of the synthesized  $\alpha$ -Fe<sub>2</sub>O<sub>3</sub> lattice obtained from XRD and HRTEM analysis.

Planar	$d_{hkl}^a$	$d$ -Spacing <sup>b</sup>
0 1 2	3.68	3.50
1 0 4	2.70	2.65
1 1 0	2.51	2.48
1 1 3	2.21	2.28

<sup>a</sup> Value obtained from XRD analysis.

<sup>b</sup> Lattice fringes obtained from HRTEM analysis.

present in the literature [25]. These peaks indicate a hematite phase of Fe<sub>2</sub>O<sub>3</sub> with rhombohedral symmetry (JCPDS file No 33-0664). The particle size of the  $\alpha$ -Fe<sub>2</sub>O<sub>3</sub> was found to be 30.2 nm as determined by the Debye–Scherrer equation (Eq. (3)), based on the major peak of  $\alpha$ -Fe<sub>2</sub>O<sub>3</sub> (1 0 4) at  $2\theta = 33.1^\circ$  (Fig. 1A),

$$\tau = \frac{k\lambda}{\beta \cos \theta} \quad (3)$$

where  $\tau$  is the particle size,  $\lambda$  is the wavelength of the X-ray radiation (Cu K $\alpha = 0.1542$  nm),  $k$  is the shape factor ( $k = 0.94$ ),  $\beta$  is the line width at half maximum height and  $\theta$  is the angular position of the peak maximum [26,27].

The XRD patterns of  $\alpha$ -Fe<sub>2</sub>O<sub>3</sub>/HY<sub>IS</sub> (Fig. 1B/c) and  $\alpha$ -Fe<sub>2</sub>O<sub>3</sub>/HY<sub>IE</sub> (Fig. 1B/d) are similar to those of HY (Fig. 1B/b), indicating that the introduction of  $\alpha$ -Fe<sub>2</sub>O<sub>3</sub> did not affect the structure of the catalyst [5,28]. However, the intensity of the peaks decreased slightly, probably due to a change in the crystallinity of the catalysts in part because of the  $\alpha$ -Fe<sub>2</sub>O<sub>3</sub> distribution on the HY surface [29]. The diffraction spectra of  $\alpha$ -Fe<sub>2</sub>O<sub>3</sub> could not be observed in either the  $\alpha$ -Fe<sub>2</sub>O<sub>3</sub>/HY<sub>IS</sub> or  $\alpha$ -Fe<sub>2</sub>O<sub>3</sub>/HY<sub>IE</sub> catalysts. Similar phenomena were reported for TiO<sub>2</sub> supported on HY and iron supported on mesoporous silica, in which the metal loading was more than 10 wt% and could only be detected by XRD [30,31].

TEM analysis was carried out to better understand the catalysts' morphology and size distribution. Fig. 2 shows TEM micrographs of HY, the synthesized  $\alpha$ -Fe<sub>2</sub>O<sub>3</sub>,  $\alpha$ -Fe<sub>2</sub>O<sub>3</sub>/HY<sub>IS</sub> and  $\alpha$ -Fe<sub>2</sub>O<sub>3</sub>/HY<sub>IE</sub>. The HRTEM image of  $\alpha$ -Fe<sub>2</sub>O<sub>3</sub> (Fig. 2a) demonstrates that the particles are irregularly shaped with sizes in the range of 20–40 nm. The interplanar spacing shown in Fig. 2b was determined to be 0.355 nm, which corresponds to the  $d$ -spacing of the (0 1 2) plane of rhombohedral Fe<sub>2</sub>O<sub>3</sub> hematite [32]. The values of the other interplanar spacings ( $d$ -spacings) of the lattice fringes in this image were found to be consistent with the  $d$ -spacings of  $\alpha$ -Fe<sub>2</sub>O<sub>3</sub> obtained from the Scherrer equation in the XRD analysis (Fig. 1A and Table 1). Compared with the translucent images of HY (Fig. 2c), the distribution of iron oxide nanoparticles on the surface of HY was clearly observed in both  $\alpha$ -Fe<sub>2</sub>O<sub>3</sub>/HY<sub>IS</sub> (Fig. 2d) and  $\alpha$ -Fe<sub>2</sub>O<sub>3</sub>/HY<sub>IE</sub> (Fig. 2e) [28]. A FESEM–EDX analysis was carried out to confirm the presence of Fe, and the results are presented in Table 2. The weight percent loadings of Fe in both  $\alpha$ -Fe/HY<sub>IS</sub> and  $\alpha$ -Fe/HY<sub>IE</sub> are both approximately 5 wt%.

Fig. 3 shows the solid reflectance UV–vis spectra of HY and the prepared catalysts. Both  $\alpha$ -Fe<sub>2</sub>O<sub>3</sub>/HY<sub>IS</sub> and  $\alpha$ -Fe<sub>2</sub>O<sub>3</sub>/HY<sub>IE</sub> displayed the characteristic peak of  $\alpha$ -Fe<sub>2</sub>O<sub>3</sub>. The band gap energies of the catalysts were determined using the Kubelka–Munk ( $K$ – $M$ ) spectrum by plotting the function  $f_{K-M} = (hc/\lambda)^2$  versus  $h\nu$  (figure not shown)

**Table 2**

FESEM–EDX of 5 wt%  $\alpha$ -Fe<sub>2</sub>O<sub>3</sub>/HY<sub>IS</sub> and 5 wt%  $\alpha$ -Fe<sub>2</sub>O<sub>3</sub>/HY<sub>IE</sub>.

Element	$\alpha$ -Fe <sub>2</sub> O <sub>3</sub> /HY <sub>IS</sub> (%)	$\alpha$ -Fe <sub>2</sub> O <sub>3</sub> /HY <sub>IE</sub> (%)
C	2.68	3.67
O	41.3	39.5
Al	0.98	1.53
Si	50.2	50.4
Fe	4.83	4.90

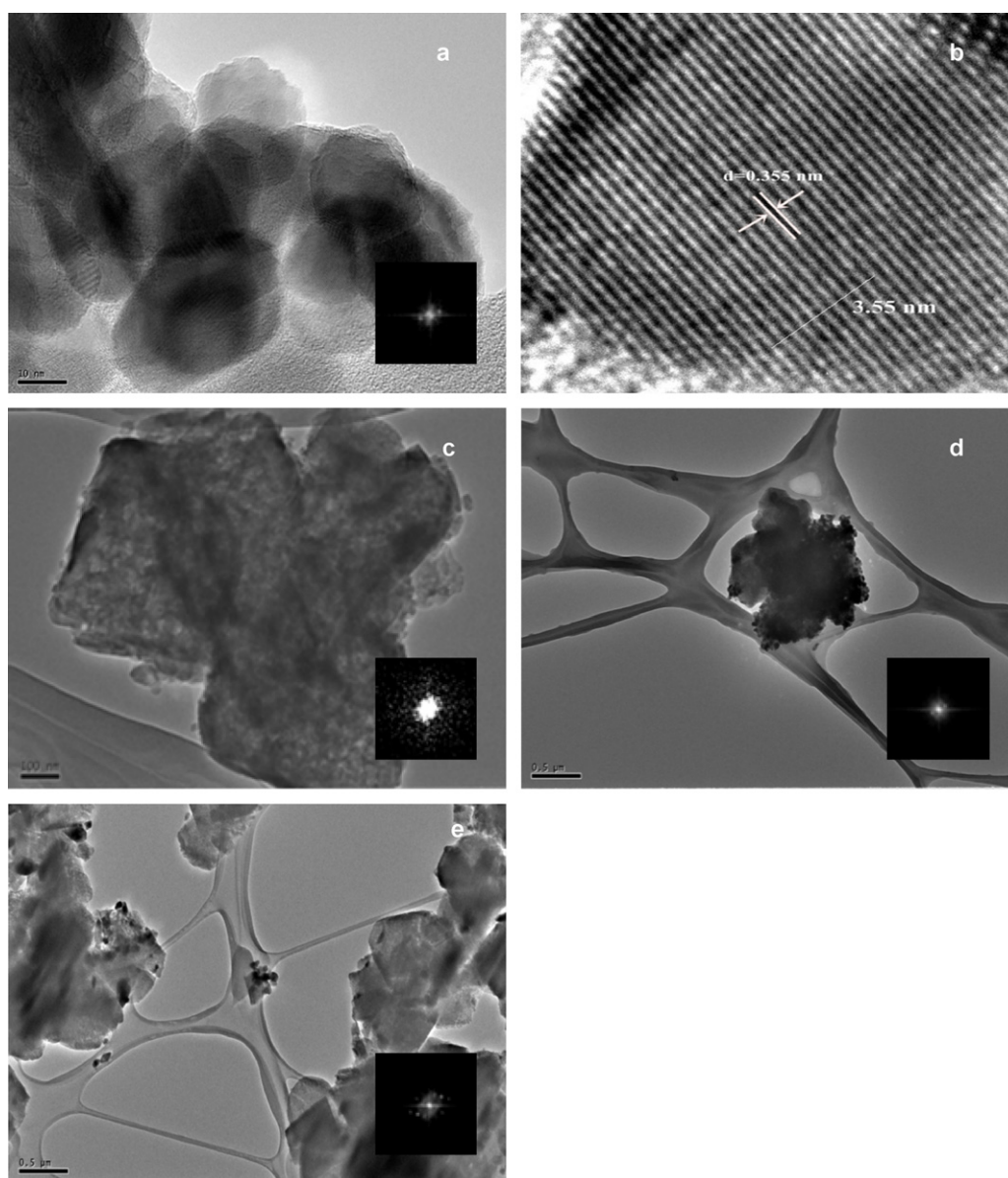
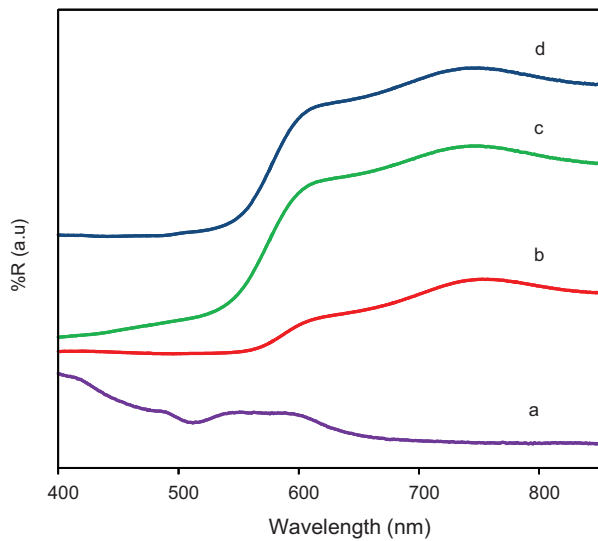


Fig. 2. HRTEM images of the photocatalysts in low and high magnification: (a and b)  $\alpha$ -Fe<sub>2</sub>O<sub>3</sub>; (c) HY; (d)  $\alpha$ -Fe<sub>2</sub>O<sub>3</sub>/HY<sub>IE</sub>; and (e)  $\alpha$ -Fe<sub>2</sub>O<sub>3</sub>/HY<sub>IS</sub>.

[33]. The band gaps of both  $\alpha$ -Fe<sub>2</sub>O<sub>3</sub>/HY<sub>IS</sub> and  $\alpha$ -Fe<sub>2</sub>O<sub>3</sub>/HY<sub>IE</sub> were estimated to be 2.1 eV, which does not differ greatly from that of the synthesized  $\alpha$ -Fe<sub>2</sub>O<sub>3</sub> (2.2 eV), and is also in agreement with the value reported in the literature [34,35]. The introduction of Fe into HY seemed to lower the band gap energy, and this result demonstrates the suitability of the system for photocatalytic reactions under visible light sources below 563 nm [36].

To study the details of the hydroxyl groups involved in the catalyst structure prepared by the different methods, the samples were evacuated at 673 K for 1 h prior to IR measurement and the results are shown in Fig. 4A. The sharp peak at 3745 cm<sup>-1</sup> could be attributed to the hydroxyl groups of the terminal and internal framework defects of the SiOH groups [37]. The peaks for both 5 wt%  $\alpha$ -Fe<sub>2</sub>O<sub>3</sub>/HY<sub>IE</sub> and 5 wt%  $\alpha$ -Fe<sub>2</sub>O<sub>3</sub>/HY<sub>IS</sub> were shifted toward the lower wavenumber of 3740 cm<sup>-1</sup>, which corresponds to the internal silanol group at the framework, indicating the possible weak interaction with the neighboring metal species [38]. A considerable increase in intensity was observed at the 3740 cm<sup>-1</sup> peak for  $\alpha$ -Fe<sub>2</sub>O<sub>3</sub>/HY<sub>IE</sub> but not for  $\alpha$ -Fe<sub>2</sub>O<sub>3</sub>/HY<sub>IS</sub> when compared with the parent HY. A peak at 3700 cm<sup>-1</sup> for both catalysts, which was

assigned to a hydroxyl group in a defect site at the HY framework, disappeared with iron loading. In addition, a broad peak at 3660 cm<sup>-1</sup> rose slightly for  $\alpha$ -Fe<sub>2</sub>O<sub>3</sub>/HY<sub>IE</sub>, which corresponded to the presence of hydroxyls in the extra framework aluminum species [37]. This result signifies the possible effect of dealumination [38]. The disappearance of the hydroxyl groups of the SiOH groups in the defect sites (3745 cm<sup>-1</sup> and 3700 cm<sup>-1</sup>) may be responsible for the formation of hydroxyls in the extra framework aluminum species. To determine the possible interaction between iron and the HY framework, the effect of iron loading was studied on  $\alpha$ -Fe<sub>2</sub>O<sub>3</sub>/HY<sub>IS</sub>, and the result is shown in Fig. 4B (region 1350–950 cm<sup>-1</sup>) and C (region 800–450 cm<sup>-1</sup>). Fig. 4B shows a sharp peak at 1080 cm<sup>-1</sup>, which might correspond to the asymmetric Si–O–Si vibration. This peak decreased with increasing iron loading, possibly indicating an Al ion exchange, instead of Fe with the silicon of the Si–O–Si groups [39]. In fact, as shown in Fig. 4C(b),  $\alpha$ -Fe<sub>2</sub>O<sub>3</sub> exhibited two broad peaks at 540 and 475 cm<sup>-1</sup>. However, no peak showing the interaction between  $\alpha$ -Fe<sub>2</sub>O<sub>3</sub> and HY was observed in Fig. 4C(c–f), possibly because the amount of iron added was very small [40].



**Fig. 3.** Solid reflectance UV-vis spectra of (a) HY; (b)  $\alpha$ -Fe<sub>2</sub>O<sub>3</sub>; (c)  $\alpha$ -Fe<sub>2</sub>O<sub>3</sub>/HY<sub>IS</sub>; and (d)  $\alpha$ -Fe<sub>2</sub>O<sub>3</sub>/HY<sub>IE</sub>.

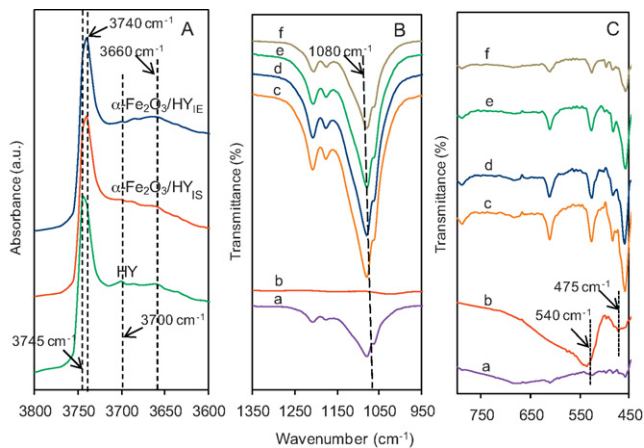


**Fig. 4.** FT-IR spectra of (A) HY and the catalysts prepared by different methods; (B and C)  $\alpha$ -Fe<sub>2</sub>O<sub>3</sub>/HY<sub>IS</sub> with various iron loadings: (a) HY, (b)  $\alpha$ -Fe<sub>2</sub>O<sub>3</sub>, (c) 2 wt%  $\alpha$ -Fe<sub>2</sub>O<sub>3</sub>/HY<sub>IS</sub>, (d) 3 wt%  $\alpha$ -Fe<sub>2</sub>O<sub>3</sub>/HY<sub>IS</sub>, (e) 5 wt%  $\alpha$ -Fe<sub>2</sub>O<sub>3</sub>/HY<sub>IS</sub>, and (f) 7.5 wt%  $\alpha$ -Fe<sub>2</sub>O<sub>3</sub>/HY<sub>IS</sub>.

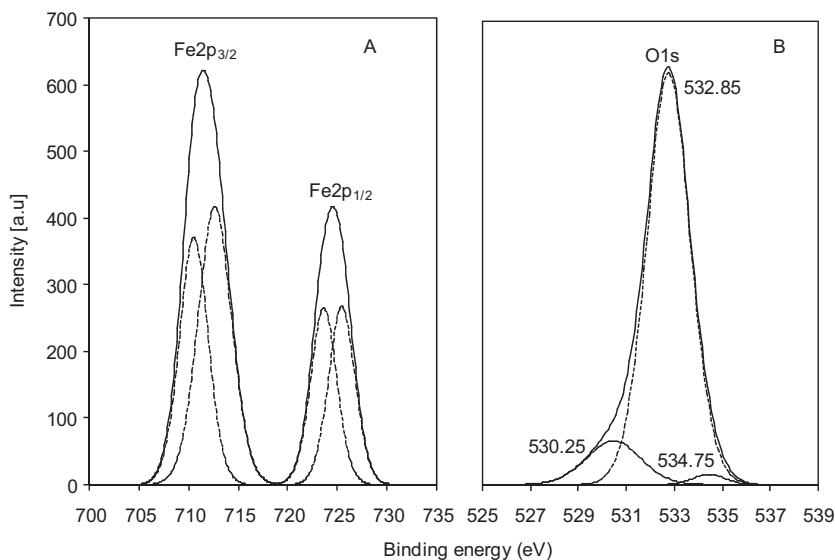


**Fig. 5.** XPS spectra of (A) Fe 2p; and (B) O 1s regions for 5 wt%  $\alpha$ -Fe<sub>2</sub>O<sub>3</sub>/HY<sub>IS</sub>.

The XPS spectrum of the  $\alpha$ -Fe<sub>2</sub>O<sub>3</sub>/HY<sub>IS</sub> in the Fe 2p and O 1s regions is shown in Fig. 5. Two peaks at 711.65 and 724.85 eV were observed in the Fe 2p spectrum, which might correspond to Fe 2p<sub>3/2</sub> and Fe 2p<sub>1/2</sub>, respectively. Both of the binding energies are similar to the reported values of 710.5 and 724.1 eV for Fe 2p in  $\alpha$ -Fe<sub>2</sub>O<sub>3</sub> [41]. However, the binding energy value of Fe 2p<sub>3/2</sub> is higher than that of bulk  $\alpha$ -Fe<sub>2</sub>O<sub>3</sub>, which is probably due to the strong interaction between iron and HY [42,43]. Furthermore, the O 1s spectrum showed the existence of shoulder peaks in addition to the main peak. The main peak at 534.75 eV is due to Si–O–H groups while the peak 532.85 eV could be due to Si–O–Si groups [44]. The existence of a peak at 530.25 eV might be due to the increase in the ionic state of the oxygen bond when some Si–O–Si groups convert to Si–O–Fe [45]. The XPS spectrum of Fe 2p and O 1s showed that the valence states of Fe and O are +3 and –2, respectively.

<sup>27</sup>Al and <sup>29</sup>Si Solid-state Magic Angle Spinning NMR (MAS NMR) analysis of the catalysts was carried out to determine the ordering of the Si and Al atoms in the HY framework, and the results are shown in Fig. 6. A sample of the parent catalyst HY was compared with both 5 wt%  $\alpha$ -Fe<sub>2</sub>O<sub>3</sub>/HY<sub>IS</sub> and 5 wt%  $\alpha$ -Fe<sub>2</sub>O<sub>3</sub>/HY<sub>IE</sub>. It is clearly observed from Fig. 6A in the <sup>29</sup>Si MAS NMR spectra that the Si(OAl) peak almost completely disappeared when the catalyst was prepared by the in situ method (for 5 wt%  $\alpha$ -Fe<sub>2</sub>O<sub>3</sub>/HY<sub>IS</sub>), but this peak in 5 wt%  $\alpha$ -Fe<sub>2</sub>O<sub>3</sub>/HY<sub>IE</sub> did not differ greatly from that of the parent catalyst. These results indicate that a possible interaction occurred between the Si(OAl) groups and iron species when the catalyst was prepared by the in situ method, but no particular reaction occurred when the catalyst was prepared by the ion-exchange method [46]. On the other hand, Fig. 6B illustrates the disappearance of the tetrahedral aluminum at peak 62 ppm, indicating that it was almost completely removed from the framework for both catalysts. A small peak is observed at 0 ppm for  $\alpha$ -Fe<sub>2</sub>O<sub>3</sub>/HY<sub>IE</sub> but not for  $\alpha$ -Fe<sub>2</sub>O<sub>3</sub>/HY<sub>IS</sub>, which corresponds to the extra-framework aluminum [47]. This result is consistent with the FTIR result of  $\alpha$ -Fe<sub>2</sub>O<sub>3</sub>/HY<sub>IE</sub>, which indicated the existence of hydroxyl group in extra framework aluminum at peak 3660 cm<sup>-1</sup>. No other significant peak was observed in Fig. 6A for either  $\alpha$ -Fe<sub>2</sub>O<sub>3</sub>/HY<sub>IS</sub> or  $\alpha$ -Fe<sub>2</sub>O<sub>3</sub>/HY<sub>IE</sub>, except the Si(OAl) peak, indicating no reinsertion of the eliminated aluminum into the Si framework (inset, Fig. 6A). Therefore, as reported by Klinowski, the eliminated aluminum from  $\alpha$ -Fe<sub>2</sub>O<sub>3</sub>/HY<sub>IS</sub> could be considered to be invisible aluminum, which might be present as Al(OH)<sub>3</sub>, Al(OH)<sup>2+</sup>, Al(OH)<sub>2</sub><sup>+</sup>, Al<sub>2</sub>O<sub>3</sub> or some other polymeric

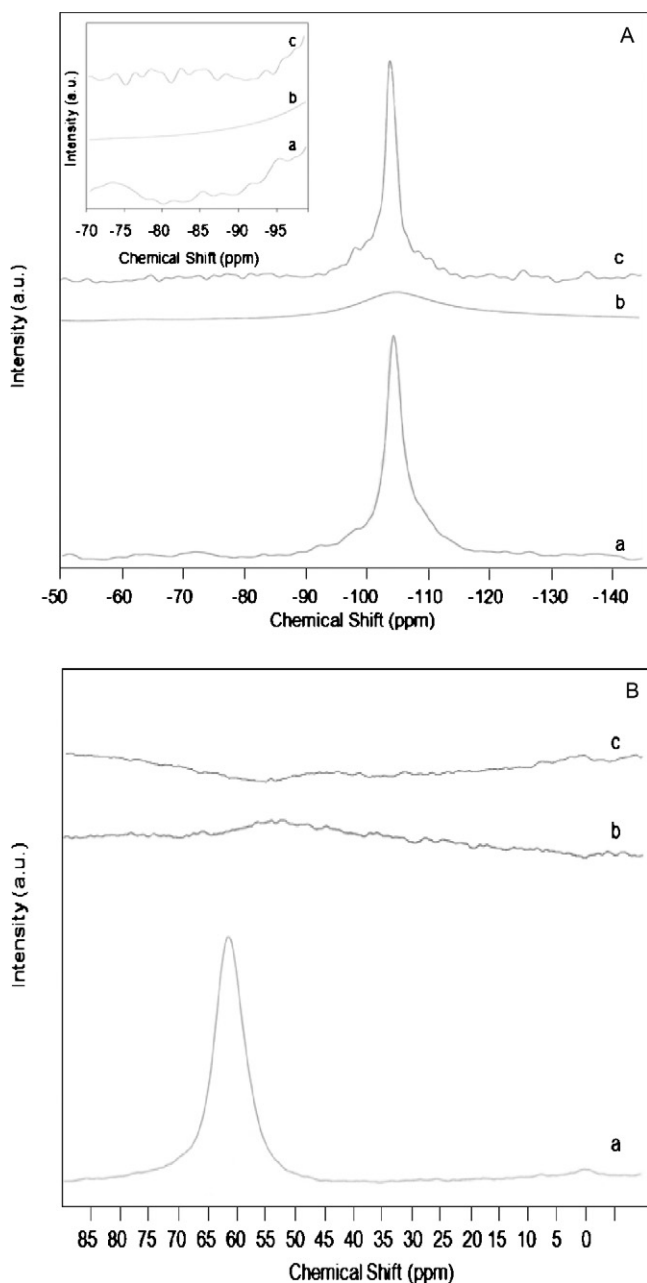
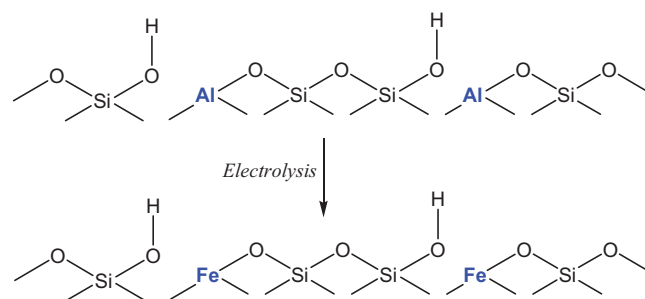


**Fig. 6.** NMR spectra of (A)  $^{29}\text{Si}$ ; and (B)  $^{27}\text{Al}$  for (a) HY, (b) 5 wt%  $\alpha\text{-Fe}_2\text{O}_3/\text{HY}_{\text{IS}}$ , and (c) 5 wt%  $\alpha\text{-Fe}_2\text{O}_3/\text{HY}_{\text{IE}}$ .

aluminous species [47]. In fact, the aluminum probably collapsed as a result of either calcination or replacement with iron during electrolysis [48]. Referring to the XPS spectra of  $\alpha\text{-Fe}_2\text{O}_3/\text{HY}_{\text{IS}}$  that show the presence of the Si—O—Fe bond, the framework vacancies created by the removal of tetrahedral aluminum may be subsequently reoccupied by iron ions during electrolysis. The disappearance of Si(OAl) peaks in Fig. 6A for  $\alpha\text{-Fe}_2\text{O}_3/\text{HY}_{\text{IS}}$  is also perhaps due to the rearrangement of the Si atoms with iron atoms in the HY framework. It is assumed that ion exchange did not occur during the preparation of  $\alpha\text{-Fe}_2\text{O}_3/\text{HY}_{\text{IE}}$  because all of the Fe cations were already reduced to Fe metals during the electrolysis prior to addition of HY into the solution [22].

From the characterization results above, a proposed molecular structure of the  $\alpha\text{-Fe}_2\text{O}_3/\text{HY}_{\text{IS}}$  is presented in Scheme 1. FTIR spectra show the possible weak interactions of the hydroxyl groups with the metal ions and the disappearance of hydroxyl groups in defect



**Scheme 1.** Proposed molecular structure of  $\alpha\text{-Fe}_2\text{O}_3/\text{HY}_{\text{IS}}$  after electrolysis.

sites. Dealumination of the  $\alpha\text{-Fe}_2\text{O}_3/\text{HY}_{\text{IS}}$  was also verified by the  $^{27}\text{Al}$  MAS NMR, while  $^{29}\text{Si}$  MAS NMR indicated the collapse of the Si(OAl) groups from the HY framework. In addition, the XPS spectrum of Fe 2p and O 1s confirmed the chemical oxidation state of the  $\text{Fe}^{3+}$  ions and the presence of the Si—O—Fe group, respectively. As a result, it could be concluded that the vacant sites created by the dealuminated Al were then filled by  $\text{Fe}^{3+}$  to form the structure as shown in Scheme 1. Remarkably, this study showed that the dealumination accompanying the ion exchange process was easily achieved by a facile electrolysis system without using any strong acids, reactive compounds and/or hydrothermal treatment [38].

### 3.2. Photocatalytic testing on the decolorization of methyl orange

#### 3.2.1. Performance of the prepared catalyst

The performance of the prepared catalysts was examined by the decolorization of MO and the results are shown in Fig. 7A. All of the catalysts,  $\alpha\text{-Fe}_2\text{O}_3$ ,  $\alpha\text{-Fe}_2\text{O}_3/\text{HY}_{\text{IS}}$  and  $\alpha\text{-Fe}_2\text{O}_3/\text{HY}_{\text{IE}}$ , were tested under both dark (dotted line) and UV-light conditions (solid line). For all the cases studied, reactions under UV-light (Fig. 7c, d and f) showed better performance compared with those conducted in the dark (Fig. 7a, b and e), indicating the necessity of light in this process. Compared with bare  $\alpha\text{-Fe}_2\text{O}_3$ , the introduction of iron into HY resulted in a higher photodecolorization percentage of MO, with the highest removal percentage of 80% being achieved when  $\alpha\text{-Fe}_2\text{O}_3/\text{HY}_{\text{IS}}$  was used. This result verifies the role of HY as a supporter for good dispersion of iron oxides compared to agglomerated bare  $\alpha\text{-Fe}_2\text{O}_3$ . However, the reaction using  $\alpha\text{-Fe}_2\text{O}_3/\text{HY}_{\text{IE}}$  only removed 23% of the MO after 2 h of contact time. Fig. 7B shows the UV-vis spectra and color change for the decolorization progress of MO by  $\alpha\text{-Fe}_2\text{O}_3/\text{HY}_{\text{IS}}$  at pH 2 for 2 h. MO shows an absorption peak at 508 nm and the decrease in the absorbance with time indicates that MO was successfully decolorized to a nearly colorless state by  $\alpha\text{-Fe}_2\text{O}_3/\text{HY}_{\text{IS}}$ .

The current research findings of various photocatalysts on the degradation of MO dye were compared and the result is tabulated in Table 3. It can be clearly observed that  $\alpha\text{-Fe}_2\text{O}_3/\text{HY}_{\text{IS}}$  is quite comparable to other metal oxide catalysts, either with or without supports. The ZnO-SnO<sub>2</sub> and SrTiO<sub>3</sub> gave higher decolorization percentages but required a high UV energy and catalyst dosage, respectively [49,50]. Supported semiconductor photocatalysts, including TiO<sub>2</sub>-SiO<sub>2</sub>, TiO<sub>2</sub>/HZSM-5 and Pt/TiO<sub>2</sub>/zeolite, also exhibit high performance but the need for higher dosages, UV energy or reaction time may limit their applications [51–53]. Thus, the lowest dosage of  $\alpha\text{-Fe}_2\text{O}_3/\text{HY}_{\text{IS}}$ , combined with a lower energy requirement and less time to decolorize a higher MO initial concentration, could be a potential alternative catalyst.

Based on the structure properties of the catalysts shown in the inset table in Fig. 8, there are no significant changes in the surface area, pore volume and pore diameter of  $\alpha\text{-Fe}_2\text{O}_3/\text{HY}_{\text{IE}}$  compared to bare HY; but,  $\alpha\text{-Fe}_2\text{O}_3/\text{HY}_{\text{IS}}$  was minimally affected. The Barret–Joyner–Halenda (BJH) pore size distribution curves

**Table 3**  
Comparison of the decolorization of MO obtained in this study with the findings in the literature.

Catalyst	Initial dye conc. (mg L <sup>-1</sup> )	Dosage (g L <sup>-1</sup> )	Light source	Contact time (min)	Decolorization (%)	Ref.
ZnO–SnO <sub>2</sub>	20	2.5	UV (300 W)	60	100	[50]
SrTiO <sub>3</sub>	10	5.0	UV (15 W)	180	98	[51]
TiO <sub>2</sub> –SiO <sub>2</sub>	20	1.0	UV (400 W)	90	93.5	[52]
TiO <sub>2</sub> /HZSM-5	10	0.5	UV (20 W)	150	99.5	[53]
Pt/TiO <sub>2</sub> /zeolite	20	2.0	UV (500 W)	30	86.2	[54]
α-Fe <sub>2</sub> O <sub>3</sub> /HY <sub>IS</sub>	30	0.38	UV (20 W)	120	80	This study

(Fig. 8) also shows a slight decrease in pore volume when iron was loaded onto HY, particularly for α-Fe<sub>2</sub>O<sub>3</sub>/HY<sub>IS</sub>, indicating a little pore blocking on both of the catalysts. Nevertheless, α-Fe<sub>2</sub>O<sub>3</sub>/HY<sub>IS</sub> demonstrated the highest decolorization rate among the catalysts in the decolorization of MO. Therefore, it can be concluded that the iron bonded to the HY framework in α-Fe<sub>2</sub>O<sub>3</sub>/HY<sub>IS</sub> (Scheme 1) plays an important role as the active species in the efficient photodecolorization of MO. In contrast, the α-Fe<sub>2</sub>O<sub>3</sub> nanoparticles that were distributed on the surface of α-Fe<sub>2</sub>O<sub>3</sub>/HY<sub>IE</sub> were not active enough to undergo similar performance as in α-Fe<sub>2</sub>O<sub>3</sub>/HY<sub>IS</sub>.

### 3.2.2. Effect of pH

The pH solution plays an important role in the photodecolorization of a dye. Semiconductor oxides usually exhibit an amphoteric behavior, which influences the surface-charge properties of the photocatalysts when the reactions occur on the surface of the semiconductor [54]. In this study, the effect of pH on the removal of MO was examined over a pH range from 2 to 11 by using both α-Fe<sub>2</sub>O<sub>3</sub>/HY<sub>IS</sub> and α-Fe<sub>2</sub>O<sub>3</sub>/HY<sub>IE</sub>. The color of MO changed from yellow to orange and then to red in acidic conditions because of the contribution of the hydrazone structure to the resonance [3]. The highest decolorization was obtained at pH 2 with a decolorization of 80% and 23% for α-Fe<sub>2</sub>O<sub>3</sub>/HY<sub>IS</sub> and α-Fe<sub>2</sub>O<sub>3</sub>/HY<sub>IE</sub>, respectively. The activities of the catalysts may have been affected by the existence of a strong electrostatic field between the positively charged catalyst surface and the negatively charged MO, as well as the activity of the Fe cations inside the framework of the zeolite [55]. Increases in the pH did not seem to favor the photodecolorization, which may be due to the reduction in the amount of positive charges on the surface of the catalyst, which in turn decreases the attraction of MO towards the surface. The reaction was not performed in alkaline conditions due to the competition between the hydroxyl ions and MO ions in the system. The same phenomenon was observed in the decolorization of Orange G by Fe–Ni nanoparticles [56].

### 3.2.3. Effect of catalyst dosage

To study the effect of catalyst dosage, a 30 mg L<sup>-1</sup> MO solution was studied at pH 2 under various catalytic doses ranging from 0.25 to 0.625 g L<sup>-1</sup>. Fig. 9 shows a plot of the decolorization percentage of MO for both α-Fe<sub>2</sub>O<sub>3</sub>/HY<sub>IS</sub> and α-Fe<sub>2</sub>O<sub>3</sub>/HY<sub>IE</sub> catalysts. The decolorization increased with increasing catalyst dosage up to

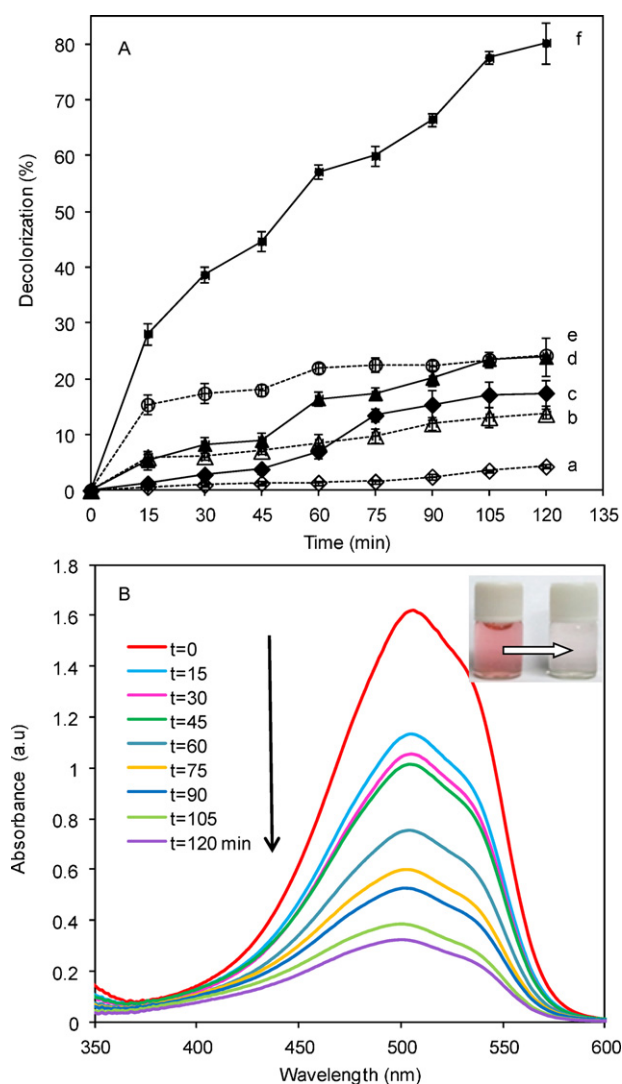


**Fig. 7.** (A) Removal of MO by various catalysts for 2 h at pH 2: (a) α-Fe<sub>2</sub>O<sub>3</sub> (dark), (b) α-Fe<sub>2</sub>O<sub>3</sub>/HY<sub>IE</sub> (dark), (c) α-Fe<sub>2</sub>O<sub>3</sub> (UV), (d) α-Fe<sub>2</sub>O<sub>3</sub>/HY<sub>IE</sub> (UV), (e) α-Fe<sub>2</sub>O<sub>3</sub>/HY<sub>IS</sub> (dark), and (f) α-Fe<sub>2</sub>O<sub>3</sub>/HY<sub>IS</sub> (UV). (B) UV-vis spectra and color change of decolorization of MO by α-Fe<sub>2</sub>O<sub>3</sub>/HY<sub>IS</sub>.

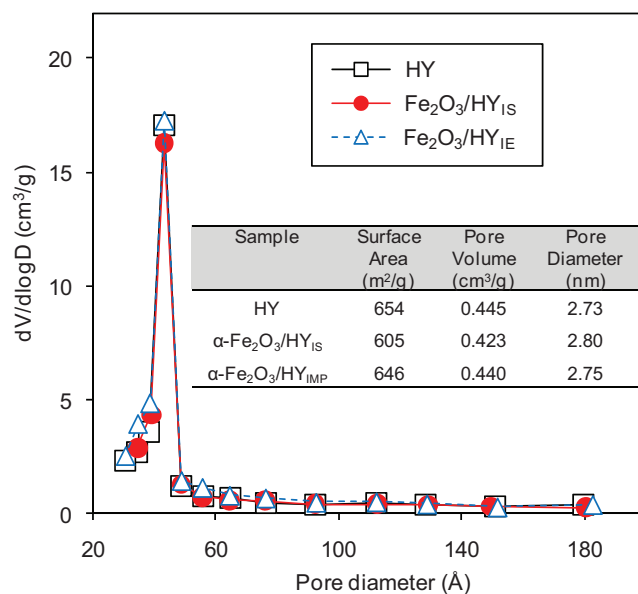


**Fig. 8.** Pore size distribution curves and structural properties of HY, 5 wt% α-Fe<sub>2</sub>O<sub>3</sub>/HY<sub>IS</sub>, and 5 wt% α-Fe<sub>2</sub>O<sub>3</sub>/HY<sub>IE</sub>. The insert table shows the textural properties of the catalysts.

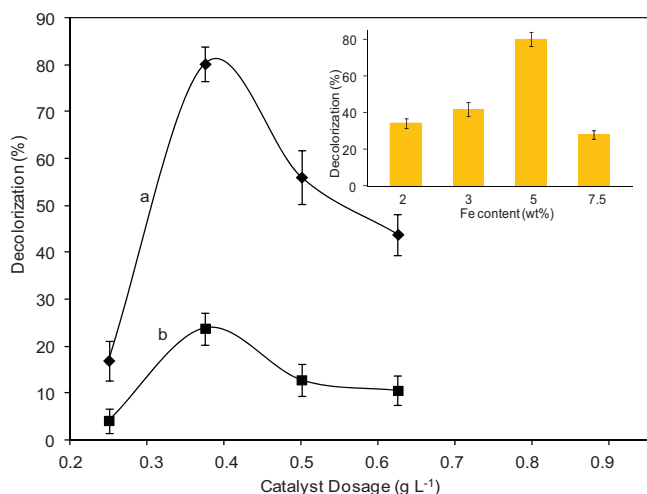


**Fig. 9.** Effect of the catalyst dosage on the decolorization of MO: (a) 5 wt%  $\alpha$ -Fe<sub>2</sub>O<sub>3</sub>/HYIS, and (b) 5 wt%  $\alpha$ -Fe<sub>2</sub>O<sub>3</sub>/HYIE. The inset highlights the effect of  $\alpha$ -Fe<sub>2</sub>O<sub>3</sub> loading for  $\alpha$ -Fe<sub>2</sub>O<sub>3</sub>/HYIS catalyst on the decolorization of MO.

0.375 g L<sup>-1</sup>, but further addition of the catalyst did not produce any significant effect on the decolorization. This result could be due to the increased turbidity of the suspension, which reduces light penetration and inhibits photodecolorization [5]. The increase in the catalyst dosage led to an increase in the active surface area and enhanced the decolorization up to 80% for  $\alpha$ -Fe<sub>2</sub>O<sub>3</sub>/HYIS [57,58]. However, the less active  $\alpha$ -Fe<sub>2</sub>O<sub>3</sub>/HYIE only gave a 23% decolorization of MO.

### 3.2.4. Effect of iron content on HY

The effect of the  $\alpha$ -Fe<sub>2</sub>O<sub>3</sub> content in HY was studied for the decolorization of MO in the range of 2–7.5 wt% loading using 0.375 g L<sup>-1</sup>  $\alpha$ -Fe<sub>2</sub>O<sub>3</sub>/HYIS for a 2 h irradiation time (inset figure in Fig. 9). The decolorization increased with the increasing iron loading up to 5 wt%, yielding a maximum decolorization percentage of 80%, but then decreased when 7.5 wt%  $\alpha$ -Fe<sub>2</sub>O<sub>3</sub> was used. Further addition of  $\alpha$ -Fe<sub>2</sub>O<sub>3</sub> most probably resulted in more agglomeration of iron oxide on the surface of HY, which then reduced the surface area for MO attraction and light penetration for an efficient photocatalytic reaction. A similar observation was reported on the photocatalytic degradation of C.I. basic violet 10 using TiO<sub>2</sub> catalysts supported by Y zeolites [5].

### 3.2.5. Effect of initial concentration

The initial concentration is a very important aspect to be considered because the photocatalytic reaction rate depends on the substrate concentration. Fig. 10 shows the effect of the initial concentration, ranging from 10 to 100 mg L<sup>-1</sup>, on the decolorization of MO using  $\alpha$ -Fe<sub>2</sub>O<sub>3</sub>/HYIS and  $\alpha$ -Fe<sub>2</sub>O<sub>3</sub>/HYIE. Both catalysts demonstrated a decrease in the decolorization with the increase in the initial concentration. The increase in the concentration of MO caused the saturation of active sites on the catalyst surface with organic species, thus reducing light penetration and subsequent hydroxyl radical formation [59,60].

### 3.2.6. Kinetic study

The kinetic decolorization of MO for both 5 wt%  $\alpha$ -Fe<sub>2</sub>O<sub>3</sub>/HYIS and 5 wt%  $\alpha$ -Fe<sub>2</sub>O<sub>3</sub>/HYIE was studied using the Langmuir–Hinshelwood (L–H) kinetic model at different initial concentrations, and the results are shown in Fig. 11a and b. The

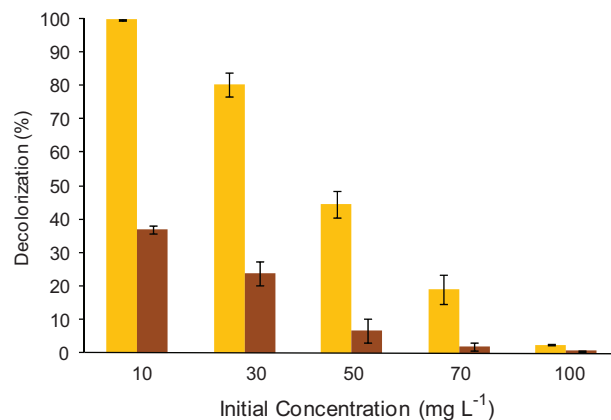


**Fig. 10.** Effect of the initial concentration on the decolorization of MO: (a) 5 wt%  $\alpha$ -Fe<sub>2</sub>O<sub>3</sub>/HYIS (yellow), and (b) 5 wt%  $\alpha$ -Fe<sub>2</sub>O<sub>3</sub>/HYIE (brown). Conditions: pH 2, 0.375 g L<sup>-1</sup> (catalyst dosage), and 2 h (irradiation time). (For interpretation of the references to color in this figure legend, the reader is referred to the web version of the article.)

line with an intercept of  $1/k_r$  and  $1/k_r K_{LH}$  was obtained from the Langmuir–Hinshelwood (L–H) kinetic formula (Eq. (4)):

$$\frac{1}{r_0} = \left[ \frac{1}{k_r K_{LH}} \right] \left[ \frac{1}{C_0} \right] + \frac{1}{k_r} \quad (4)$$

where  $r_0$  is the initial reaction rate,  $k_r$  is the reaction rate constant (mg L<sup>-1</sup> min<sup>-1</sup>),  $K_{LH}$  is the adsorption coefficient of the reactant (L mg<sup>-1</sup>) and  $C_0$  is the initial concentration of MO (mg L<sup>-1</sup>). The calculated values of  $k_r$  and  $K_{LH}$  were 1.0748 mg L<sup>-1</sup> min<sup>-1</sup> and 0.0915 L mg<sup>-1</sup>, respectively, for 5 wt%  $\alpha$ -Fe<sub>2</sub>O<sub>3</sub>/HYIS, while these values were 0.0839 mg L<sup>-1</sup> min<sup>-1</sup> and 0.0628 L mg<sup>-1</sup> for 5 wt%  $\alpha$ -Fe<sub>2</sub>O<sub>3</sub>/HYIE. The values of  $k_r$  were greater than those of  $K_{LH}$  for both catalysts, indicating the dye adsorption was the controlling step of the process. A similar phenomenon was reported on the degradation of Orange G using nano-sized Sn (IV)/TiO<sub>2</sub>/AC as a photocatalyst [61].

### 3.2.7. Effect of temperature

It was reported that semiconductor photocatalysis is usually not very temperature dependent. Nevertheless, an increase in temperature assisted the reaction to compete more efficiently with electron hole recombination [62]. In this study, the effect of temperature on the photocatalytic decolorization of MO was tested for both catalysts in the range of 303–323 K. From the Arrhenius equation, a linear plot of  $\ln k_{app}$  and  $1/T$  would give an apparent activation energy ( $E_a$ , J mol<sup>-1</sup>) [63],

$$\ln k_{app} = -\frac{E_a}{R} \frac{1}{T} + \ln A \quad (5)$$

where  $k_{app}$  (h<sup>-1</sup>) is the apparent rate constant,  $A$  is the frequency factor,  $R$  is the gas constant (8.314 J K mol<sup>-1</sup>) and  $T$  is the solution temperature (K). It was observed from the inset table in Fig. 12a and b that  $k_{app}$  for both catalysts, which was defined from the pseudo-first order plot, increased with increasing temperature. The calculated  $E_a$  for 5 wt%  $\alpha$ -Fe<sub>2</sub>O<sub>3</sub>/HYIS (Fig. 12a) and 5 wt%  $\alpha$ -Fe<sub>2</sub>O<sub>3</sub>/HYIE (Fig. 12b) are 45.8 kJ mol<sup>-1</sup> and 70.2 kJ mol<sup>-1</sup>, respectively, signifying the effectiveness of 5 wt%  $\alpha$ -Fe<sub>2</sub>O<sub>3</sub>/HYIS compared to 5 wt%  $\alpha$ -Fe<sub>2</sub>O<sub>3</sub>/HYIE in this study.

### 3.2.8. Proposed reaction mechanism for the photodecolorization of MO

The above results verify that the incorporation of  $\alpha$ -Fe<sub>2</sub>O<sub>3</sub> and HY have a significant role in enhancing the decolorization of MO. The presence of Fe<sup>3+</sup> species was confirmed by XPS (Fig. 5), as well as by ESR analysis, which showed a spectral peak centered at  $g \approx 2.04$

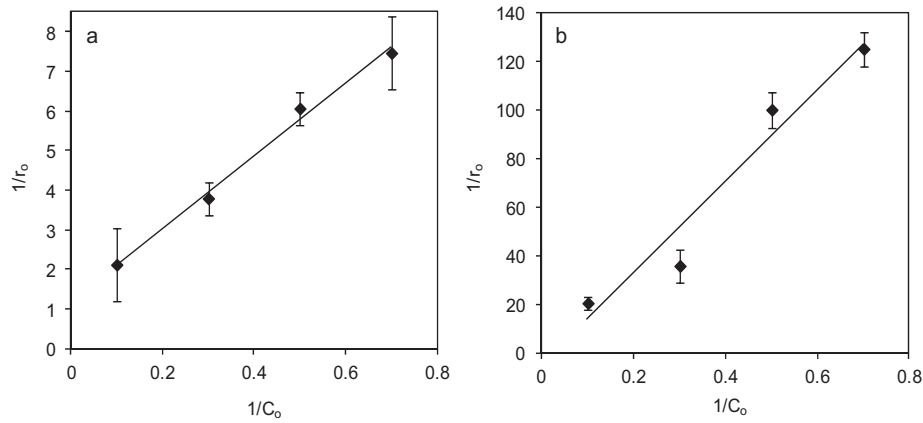
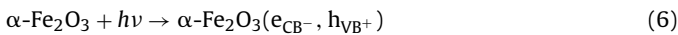
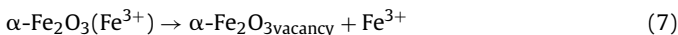


Fig. 11. Relationship between  $1/r_0$  and  $1/C_0$  at different concentrations of MO: (a) 5 wt%  $\alpha\text{-Fe}_2\text{O}_3/\text{HY}_{1\text{S}}$ ; and (b) 5 wt%  $\alpha\text{-Fe}_2\text{O}_3/\text{HY}_{1\text{E}}$ .

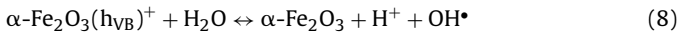
[64]. As shown in Eq. (5),  $\alpha\text{-Fe}_2\text{O}_3$  generates conduction band electrons ( $e_{\text{CB}}^-$ ) and valence band holes ( $h_{\text{VB}}^+$ ) when irradiated by a visible light energy equal to or greater than its band gap ( $E_g = 2.2$  eV) [56].



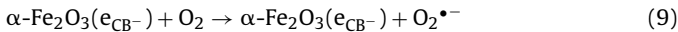
Ferric ions are also crucial species for subsequent reaction,



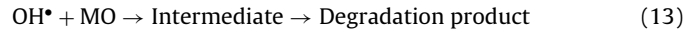
When the valence band hole ( $h_{\text{VB}}^+$ ) potential is sufficiently positive, it generates hydroxyl radicals by oxidizing water on the surface of the catalyst to  $\text{H}^+$ ,  $\text{OH}^-$  and  $\text{OH}^\bullet$  [59].



The conduction band electrons also reduce  $\text{O}_2$  on the catalyst surface to form the superoxide radical anion,  $\text{O}_2^{\bullet-}$  (Eq. (9)). The existence of these radicals may form hydrogen peroxide (Eq. (10)) or organic peroxide (Eq. (12)).



Thus, the generated hydroxyl radicals act as strong oxidizing agents that are responsible for attacking MO to form intermediates before producing degradation products.



### 3.2.9. Leaching and reusability of the photocatalyst

To study the possible leaching of iron from the catalyst into the solution, samples of experiments conducted for 2 h in the dark and for 1 and 2 h under irradiated fluorescent were subjected to AAS. The amount of Fe ions was found to be  $<0.7$   $\text{mg L}^{-1}$  (less than 1%), as tabulated in the inset table in Fig. 13, which is below the permissible level as also reported in other studies [65,66]. This indicates that the photocatalysis is mainly due to Fe present on the catalyst surface rather than the trace amount of leached Fe ions.

The stability of the photocatalyst is significant for its assessment and application. A repeated experiment was carried out with 5 wt%  $\alpha\text{-Fe}_2\text{O}_3/\text{HY}_{1\text{S}}$  in order to study the stability of the catalyst for MO decolorization (Fig. 13). The initial concentration of MO was kept constant ( $30$   $\text{mg L}^{-1}$ ) at pH 2 for 2 h irradiation time, then the catalyst was recycled after filtration and calcination at  $550^\circ\text{C}$  for 3 h at every cycle. It was observed that after five repeated experiments, the catalyst was still active, with a slight decrease in the decolorization percentage from 80% to 71.2%. The heat treatment most

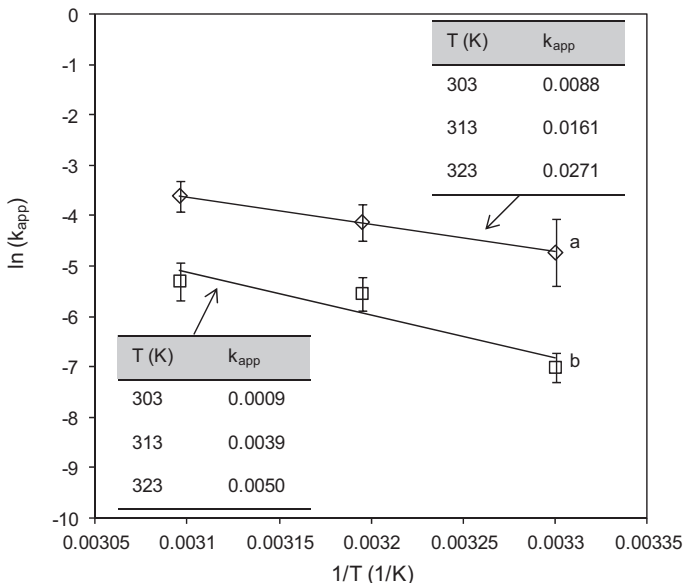


Fig. 12. Effect of reaction temperature on the pseudo-first order rate constant: (a) 5 wt%  $\alpha\text{-Fe}_2\text{O}_3/\text{HY}_{1\text{S}}$ ; (b) 5 wt%  $\alpha\text{-Fe}_2\text{O}_3/\text{HY}_{1\text{E}}$ .

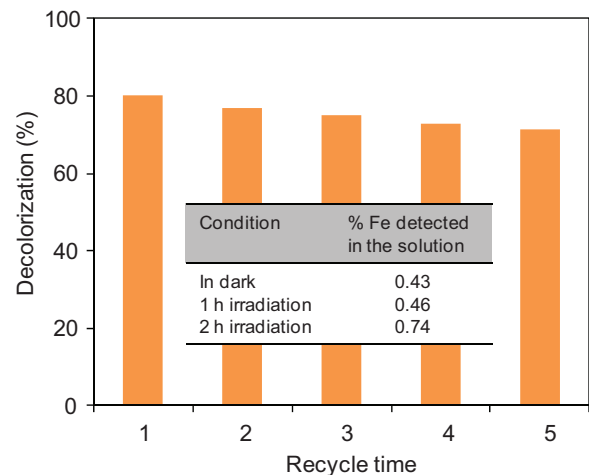
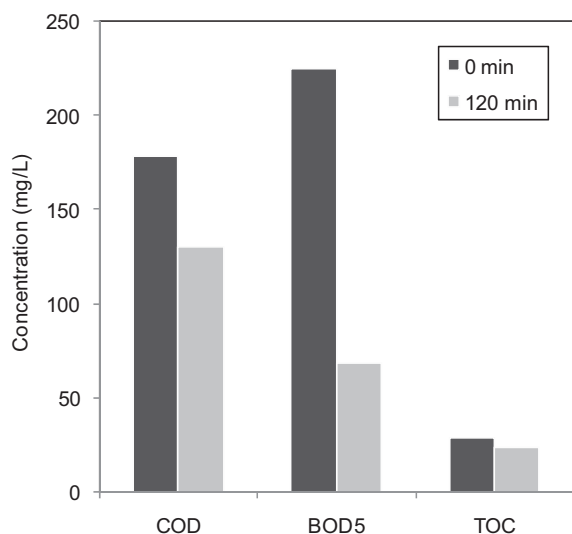


Fig. 13. Reusability of 5 wt%  $\alpha\text{-Fe}_2\text{O}_3/\text{HY}_{1\text{S}}$  on the photocatalytic decolorization of MO. Conditions: pH 2,  $0.375$   $\text{g L}^{-1}$  (catalyst dosage),  $30$   $\text{mg L}^{-1}$  (initial concentration), and 2 h (irradiation time). The inset table shows Fe leaching in the solution during experiment determined by AAS.



**Fig. 14.** BOD<sub>5</sub>, COD and TOC levels after 2 h of reaction. Conditions: pH 2, 0.375 g L<sup>-1</sup> α-Fe<sub>2</sub>O<sub>3</sub>/HY<sub>IS</sub>, and 30 mg L<sup>-1</sup> (initial concentration).

probably induced the catalyst aggregation after several recycles, which resulted in the decrease of surface area, finally leading to the decrease in photocatalytic efficiency [53]. Therefore, it can be concluded that α-Fe<sub>2</sub>O<sub>3</sub>/HY<sub>IS</sub> is a stable photocatalyst, such that deactivation did not occur during decolorization.

### 3.2.10. Investigation on biodegradability

The degree of mineralization during photocatalytic decolorization was determined in order to confirm if the final solution of MO was less toxic than the initial solution. COD, BOD<sub>5</sub> and TOC analysis are used to monitor the mineralization of the dyes [67,68]. Fig. 14 shows the COD, BOD<sub>5</sub> and TOC levels of MO solutions with 5 wt% α-Fe<sub>2</sub>O<sub>3</sub>/HY<sub>IS</sub>. The results indicate the COD, BOD<sub>5</sub> and TOC levels decreased to 27.0%, 69.6% and 16.9%, respectively, after 2 h of irradiation time. Only a slight reduction in COD and TOC were observed, although the treated MO solutions were almost colorless. As reported in several literatures, this may be due to the color removal of dye occurring faster than COD and TOC removal because of the formation of stable intermediate products, which require a longer time for further oxidation [69,70]. The cleavage of azo group –N=N– connecting two aromatic rings of MO might convert to benzene sulfonic acid, aniline, benzene or phenol [71,72]. A significant change in BOD<sub>5</sub> demonstrates that the biodegradability of the MO solution can be enhanced by this photo-oxidation system, by converting the non-biodegradable organics into biodegradable forms. In addition, the BOD<sub>5</sub>/COD ratio after 2 h of irradiation was 0.523, indicating that some non-biodegradable organic part of the MO molecule was destroyed, decomposed and even mineralized in the photocatalytic process during the irradiation time [73].

## 4. Conclusion

Nanosized α-Fe<sub>2</sub>O<sub>3</sub> supported HY zeolite (α-Fe<sub>2</sub>O<sub>3</sub>/HY) catalysts were prepared by the in situ (α-Fe<sub>2</sub>O<sub>3</sub>/HY<sub>IS</sub>) and ion-exchange (α-Fe<sub>2</sub>O<sub>3</sub>/HY<sub>IE</sub>) methods. The physicochemical properties of the catalyst were studied via XRD, FESEM-EDX, TEM, UV–vis DRS, FTIR, XPS, <sup>29</sup>Si and <sup>27</sup>Al MAS NMR and ESR. The dealumination process was easily achieved through a facile electrolysis system by replacing Al in the HY zeolite framework with Fe<sup>3+</sup> ions, and this active species was found to enhance the photodecolorization of MO. The catalyst prepared by the in situ method exhibited a better performance than the catalyst prepared by the ion-exchange method in the photodecolorization of 30 mg L<sup>-1</sup> MO; photodecolorization

percentages of 80% and 23% were obtained for 5 wt% α-Fe<sub>2</sub>O<sub>3</sub>/HY<sub>IS</sub> and 5 wt% α-Fe<sub>2</sub>O<sub>3</sub>/HY<sub>IE</sub>, respectively. The kinetic studies showed that the reaction rate is pseudo-first order as determined by the Langmuir Hinshelwood model. In addition, the activation energies (*E<sub>a</sub>*) calculated for both 5 wt% α-Fe<sub>2</sub>O<sub>3</sub>/HY<sub>IS</sub> and 5 wt% α-Fe<sub>2</sub>O<sub>3</sub>/HY<sub>IE</sub> were 45.8 kJ mol<sup>-1</sup> and 70.2 kJ mol<sup>-1</sup>, respectively. The presence of Fe<sup>3+</sup> species in the catalyst help in the formation of superoxide radical anions (O<sub>2</sub><sup>•-</sup>), which play an important role in the formation of hydroxyl radicals (OH<sup>•</sup>), a strong oxidizing agent responsible for attacking MO to form intermediates prior to producing the final degradation products. The COD, BOD<sub>5</sub> and TOC levels, used to determine the mineralization of MO, were 27.0%, 69.6% and 16.9%, respectively, after 2 h of contact time. Insignificant leaching of Fe (<1%) from the catalyst was determined by AAS. The efficiency and stability of the α-Fe<sub>2</sub>O<sub>3</sub>/HY<sub>IS</sub> catalyst prepared by a facile method was established through reusability studies that confirmed its potential as photocatalyst for the decolorization of various dyes wastewater.

## Acknowledgements

The authors are grateful for the financial support of the Research University Grant from Universiti Teknologi Malaysia (Grant No. 01H59), the awards of the MyMaster Scholarship (Nur Farhana Jaafar) from Ministry of Science, Technology and Innovation Malaysia, the support of the Hitachi Scholarship Foundation and the support and advice of Dr. Nobuhito Kurono from Hokkaido University.

## References

- [1] M. Muruganandham, N. Shobana, M. Swaminathan, Optimization of solar photocatalytic of reactive Yellow 14 azo dye in aqueous TiO<sub>2</sub>, *J. Mol. Catal.* 246 (2006) 154–161.
- [2] H. Zollinger, *Textile Chem. Color.* 23 (12) (1991) 19.
- [3] A.J. Aishah, T. Sugeng, S.H. Adam, N.D. Rahim, M.A.A. Aziz, N.H.H. Hairom, N.A.M. Razali, M.A.Z. Abidin, M.K.A. Mohamadiah, Adsorption of methyl orange from aqueous solution onto calcined lapindo volcanic mud, *J. Hazard. Mater.* 181 (2010) 755–762.
- [4] K.T. Chung, The significance of azo-reduction in the mutagenesis and carcinogenesis of azo dyes, *Mutat. Res.* 114 (April (3)) (1983) 269–281.
- [5] C.C. Wang, C.K. Lee, M.D. Lyu, L.C. Juang, Photocatalytic degradation of C.I. basic violet 10 using TiO<sub>2</sub> catalysts supported by Y zeolite: an investigation of the effects of operational parameters, *Dyes Pigments* 76 (2008) 817–824.
- [6] G. Petzold, S. Schwarz, M. Mende, W. Jaeger, Dye flocculation using polyampholytes and polyelectrolyte-surfactant nanoparticles, *J. Appl. Polym. Sci.* 104 (2007) 1342–1349.
- [7] P.K. Malik, Dye removal from wastewater using activated carbon developed from sawdust: adsorption equilibrium and kinetics, *J. Hazard. Mater.* B113 (2004) 81–88.
- [8] X.J. Lu, B. Yang, J.H. Chen, R. Sui, Treatment of wastewater containing azo dye reactive brilliant Red X-3B using sequential ozonation and up flow biological aerated filter process, *J. Hazard. Mater.* 161 (2009) 234–241.
- [9] H. Hassan, B.H. Hameed, Fe-clay as effective heterogeneous Fenton catalyst for the decolorization of Reactive Blue 4, *Chem. Eng. J.* 171 (2011) 912–918.
- [10] D. Nidhi, S.R. Sadhana, K.L. Nitin, R.N. Rashmi, V.C. Ravikrishna, D. Sukumar, Photocatalytic properties of zeolite-based materials for photoreduction of methyl orange, *Appl. Catal. A: Gen.* 202 (2006) 152–157.
- [11] D.W. Bahnemann, in: E. Pelizzetti, M. Schiavello (Eds.), *Photochemical Conversion and Storage of Solar Energy*, Kluwer Academic Publishers, Dordrecht, 1991, pp. 251–276.
- [12] J. Bandara, U. Klehm, J. Kiwi, Raschig rings-Fe<sub>2</sub>O<sub>3</sub> composite photocatalyst activate in the degradation of 4-chlorophenol and Orange II under daylight irradiation, *Appl. Catal. B: Environ.* 76 (2007) 73–81.
- [13] M. Aleksić, H. Kušić, N. Koprivanac, D. Leszczynska, A.L. Božić, Heterogeneous Fenton type processes for the degradation of organic dye pollutant in water: the application of zeolite assisted AOPs, *Desalination* 257 (2010) 22–29.
- [14] R. Prihodko, I. Stolyarova, G. Gündüz, O. Taran, S. Yasnik, V. Parmon, V. Goncharuk, Fe-exchanged zeolites as materials for catalytic wet peroxide oxidation: degradation of Rodamine G dye, *Appl. Catal. B: Environ.* 104 (2011) 201–210.
- [15] F. Chen, Y. Li, W. Cai, J. Zhang, Preparation and sono-Fenton performance of 4A-zeolite supported α-Fe<sub>2</sub>O<sub>3</sub>, *J. Hazard. Mater.* 177 (2010) 739–743.
- [16] S. Papić, N. Koprivanac, A.L. Božić, D. Vujević, S.K. Dragičević, H. Kušić, I. Peterneel, Advanced oxidation processes in azo dye wastewater treatment, *Water Environ. Res.* 78 (2006) 572–579.

- [17] F. Duarte, L.M. Madeira, Fenton- and photo-Fenton-like degradation of a textile dye by heterogeneous processes with Fe/ZSM-5 zeolite, *Sep. Sci. Technol.* 45 (2010) 1512–1520.
- [18] M. Dükkancı, G. Gündüz, S. Yılmaz, Y.C. Yaman, R.V. Prihod'ko, I.V. Stolyarova, Characterization, Catalytic activity of CuFeZSM-5 catalysts for oxidative degradation of Rhodamine 6G in aqueous solutions, *Appl. Catal. B: Environ.* 95 (2010) 270–278.
- [19] M. Dükkancı, G. Gündüz, S. Yılmaz, R.V. Prihod'ko, Heterogeneous Fenton-like degradation of Rhodamine 6G in water using CuFeZSM-5 zeolite catalyst prepared by hydrothermal synthesis, *J. Hazard. Mater.* 181 (2010) 343–350.
- [20] E. Bolova, G. Gündüz, M. Dükkancı, S. Yılmaz, Y.C. Yaman, Fe containing ZSM-5 zeolite as catalyst for wet peroxide oxidation of Orange II, *Int. J. Chem. React. Eng.* 9 (2011), Note S1.
- [21] J. Chen, L. Zhu, Heterogeneous UV-Fenton catalytic degradation of dye stuff in water with hydroxyl-Fe pillared bentonite, *Catal. Today* 126 (2007) 463–470.
- [22] A.J. Aishah, N. Kuroko, M. Tokuda, Facile synthesis of ethyl 2-arylpropenoates by cross-coupling reaction using electrogenerated highly reactive zinc, *Tetrahedron* 58 (2002) 7477–7484.
- [23] T. Sugeng, A.J. Aishah, M. Malik, Generation of protonic acid sites from pentane on the surfaces of Pt/SO<sub>4</sub><sup>2-</sup>-ZrO<sub>2</sub> and Zn/H-ZSM5 evidenced by IR study of adsorbed pyridine, *Appl. Catal. A: Gen.* 372 (2010) 90–93.
- [24] A.J. Aishah, T. Sugeng, N.A.M. Razali, N.H.H. Hairom, A. Idris, M.N.M. Muhiid, A. Ismail, N.A.M. Yahaya, N.A.L. Ahmad, H. Dzinun, Complete electrochemical dechlorination of chlorobenzenes in the presence of various arene mediators, *J. Hazard. Mater.* 174 (2010) 581–585.
- [25] Z. Zhang, M.H. Faruk, T. Takahashi, Self-assembled hematite ( $\alpha$ -Fe<sub>2</sub>O<sub>3</sub>) nanotube arrays for photoelectrocatalytic degradation of azo dye under simulated solar light irradiation, *Appl. Catal. B: Environ.* 95 (2010) 423–429.
- [26] Z. Qinghong, G. Lian, G. Jingkun, B. McKinney, M. Rouse, *Appl. Catal. B* 26 (2000) 207–215.
- [27] N. Yoshio, K. Mitsuo, N. Junichi, *J. Phys. Chem. B* 102 (1998) 10279–10283.
- [28] B. Dutta, S. Jana, A. Bhattacharjee, P. Gütllich, S.I. Iijuma, S. Koner,  $\gamma$ -Fe<sub>2</sub>O<sub>3</sub> nanoparticle in NaY-zeolite matrix: preparation, characterization, and heterogeneous catalytic epoxidation of olefins, *Inorg. Chim. Acta* 363 (2010) 696–704.
- [29] N. An, Q. Yu, Gang Liu, S. Li, M. Jia, W. Zhang, Complete oxidation of formaldehyde at ambient temperature over supported Pt/Fe<sub>2</sub>O<sub>3</sub> catalysts prepared by colloid-deposition method, *J. Hazard. Mater.* 186 (2011) 1392–1397.
- [30] H. Chen, A. Matsumoto, N. Nishimiya, K. Tsutsumi, Preparation, Characterization of TiO<sub>2</sub> incorporated Y-zeolite, *Colloid Surf. A* 157 (1999) 295–305.
- [31] X. Wang, Q. Zhang, S. Yang, Y. Wang, Iron-catalyzed propylene epoxidation by nitrous oxide: studies on the effect of alkali metal salts, *J. Phys. Chem. B* 109 (2005) 23500–23508.
- [32] M.V. Reddy, T. Yu, C.H. Sow, Z.X. Shen, C.T. Lim, G.V.S. Rao, B.V.R. Chowdar,  $\alpha$ -Fe<sub>2</sub>O<sub>3</sub> nanoflakes as an anode material for Li-ion batteries, *Adv. Funct. Mater.* 17 (2007) 2792–2799.
- [33] H. Jia, H. Xu, Y. Hu, Y. Tang, L. Zhang, TiO<sub>2</sub>/CdS core-shell nanorods films: fabrication and dramatically enhanced photoelectrochemical properties, *Electrochem. Commun.* 9 (2007) 354–360.
- [34] A. Boudjemaa, S. Boumaza, M. Trari, R. Bouarab, A. Bouguelia, Physical, Photoelectrochemical characterizations of  $\alpha$ -Fe<sub>2</sub>O<sub>3</sub>: appl. for hydrogen production, *Int. J. Hydrogen Energy* 34 (2009) 4268–4274.
- [35] S.K. Apte, S.D. Naik, R.S. Sonawane, B.B. Kale, J.O. Baeg, Synthesis of nanosized structure  $\alpha$ - and  $\gamma$ -Fe<sub>2</sub>O<sub>3</sub> and its photocatalytic activity, *J. Am. Ceram. Soc.* 90 (2007) 412–414.
- [36] C. Karunakaran, S. Senthilvelan, Fe<sub>2</sub>O<sub>3</sub>-photocatalysis with sunlight and UV light: oxidation of aniline, *Electrochem. Commun.* 8 (2006) 95–101.
- [37] A.A. Gabrienko, I.G. Danilova, S.S. Arzumyanov, A.V. Toktarev, D. Freude, A.G. Stepanov, Strong acidity of silanol groups of zeolite beta: evidence from the studies by IR spectroscopy of adsorbed CO and <sup>1</sup>H MAS NMR, *Microporous Mesoporous Mater.* 131 (2010) 210–216.
- [38] S. Krijnen, Titanium Epoxidation Catalysts: Zeolite and Silsesquioxane Based Materials, Eindhoven University of Technology, Netherlands, 1998.
- [39] H.D. Lutz, J. Henning, H. Haeuseler, A new interpretation of the frequency shifting of the OH stretching modes in solid hydroxides, *J. Mol. Struct.* 156 (1987) 143–145.
- [40] C. Wang, H. Shi, Y. Li, Synthesis, Characteristic of natural zeolite supported Fe<sup>3+</sup>-TiO<sub>2</sub> photocatalyst, *Appl. Surf. Sci.* 257 (2011) 6873–6877.
- [41] T. Tittabut, W. Trakarnpruk, Metal-loaded MgAl oxides for transesterification of glyceryl tributyrat and palm oil, *Ind. Eng. Chem. Res.* 47 (2008) 2176–2181.
- [42] K. Hirokawa, M. Oku, Application of ESCA to semi-quantitative surface and state analysis of iron oxides, *Talanta* 26 (1979) 855–859.
- [43] R.B. Borade, A. Adnot, S. Kaliaguine, Acid sites in Al-ZSM-22 and Fe-ZSM-22, *Zeolites* 17 (1991) 710–719.
- [44] M. Shimokawabe, T. Chaki, S. Ozawa, M. Arai, Activity, Physicochemical properties of Fe-zeolite catalysts for SCR of N<sub>2</sub>O with CH<sub>4</sub>, *React. Kinet. Catal. Lett.* 86 (2005) 363–370.
- [45] Y.H. Kim, D.K. Lee, H.G. Cha, C.W. Kim, Y.C. Kang, Y.S. Kang, Preparation, Characterization of the antibacterial Cu nanoparticle formed on the surface of SiO<sub>2</sub> nanoparticles, *J. Phys. Chem. B* 110 (2006) 24923–24928.
- [46] V. Simon, D. Eniu, A. Takács, K. Magyar, M. Neumann, S. Simon, Iron doping effect on the electronic structure in yttrium aluminosilicate glasses, *J. Non-Cryst. Solids* 351 (2005) 2365–2372.
- [47] J. Klinowski, Nuclear magnetic resonance studies of zeolites, *Prog. Nucl. Magn. Reson. Spectrosc.* 16 (1984) 237–309.
- [48] H. Hamdan, J. Klinowski, Isomorphous substitution of framework silicon by aluminium in silicalite: factors determining resolution of <sup>29</sup>Si magic-angle-spinning NMR spectra of pentasil zeolites, *Chem. Phys. Lett.* 139 (1987) 6–9.
- [49] C. Wang, X. Wang, B.Q. Xu, J. Zhao, B. Mai, P. Peng, G. Sheng, J. Fu, Enhanced photocatalytic performance of nanosized coupled ZnO/SnO<sub>2</sub> photocatalysts for methyl orange degradation, *J. Photochem. Photobiol. A: Chem.* 168 (2004) 47–52.
- [50] T. Puangpetch, T. Sreethawong, S. Yoshikawa, S. Chavadej, Synthesis, Photocatalytic activity in methyl orange degradation of mesoporous-assembled SrTiO<sub>3</sub> nanocrystals prepared by sol-gel method with the aid of structure-directing surfactant, *J. Mol. Catal. A: Chem.* 287 (2008) 70–79.
- [51] Y. Guo, S. Yang, X. Zhou, C. Lin, Y. Wang, W. Zhang, Enhanced photocatalytic activity for degradation of methyl orange over silica-titania, *J. Nanomater.* (2011) 1–9, Article ID 296953.
- [52] W. Zhang, K. Wang, Y. Yu, H. He, TiO<sub>2</sub>/HZSM-5 nano-composite photocatalyst: HCl treatment of NaZSM-5 promotes photocatalytic degradation of methyl orange, *Chem. Eng. J.* 163 (2010) 62–67.
- [53] M. Huang, C. Xu, Z. Wu, Y. Huang, J. Lin, J. Wu, Photocatalytic discolorization of methyl orange solution by Pt modified TiO<sub>2</sub> loaded on natural zeolite, *Dyes Pigments* 77 (2008) 327–334.
- [54] M.A. Behnajady, N. Modirshala, R. Hamzavi, Kinetic study on photocatalytic degradation of C.I. Acid Yellow 23 by ZnO photocatalyst, *J. Hazard. Mater. B* 133 (2006) 226–232.
- [55] M.B. Kasiri, H. Aleboeyeh, A. Aleboeyeh, Degradation of acid Blue 74 using Fe-HZSM5 zeolite as a heterogenous photo-Fenton catalyst, *Appl. Catal. B: Environ.* 84 (2008) 9–15.
- [56] A.D. Bokare, R.C. Chikate, C.V. Rode, K.M. Paknikar, Iron-nickel bimetallic nanoparticles for reductive degradation of azo dye Orange G in aqueous solution, *Appl. Catal. B: Environ.* 79 (2008) 270–278.
- [57] M.M. El-Moselhy, Photo-degradation of acid Red 44 using Al and Fe modified silicates, *J. Hazard. Mater.* 169 (2009) 498–508.
- [58] C.Y. Chen, Photocatalytic degradation of azo dye reactive Orange 16 by TiO<sub>2</sub>, *Water Air Soil Pollut.* 202 (2009) 335–342.
- [59] I. Poullos, I. Tsachpinis, Photodegradation of the textile dye reactive black 5 in the presence of semiconductor oxides, *J. Chem. Technol. Biotechnol.* 74 (1999) 349–357.
- [60] N. Daneshvar, D. Salari, A.R. Khataee, Photocatalytic degradation of azo dye acid Red 14 in water: investigation of the effect of operational parameters, *J. Photochem. Photobiol. A: Chem.* 157 (2003) 111–116.
- [61] J. Sun, X. Wang, J. Sun, R. Sun, L. Qiao, Photocatalytic degradation and kinetic of Orange G using nano-sizes Sn(IV)/TiO<sub>2</sub>/AC photocatalyst, *J. Mol. Catal. A: Chem.* 260 (2006) 241–246.
- [62] N. Daneshvar, M. Rabbani, N. Modirshahla, M.A. Behnajady, Kinetic modeling of photocatalytic degradation of acid Red 27 in UV/TiO<sub>2</sub> process, *J. Photochem. Photobiol. A: Chem.* 168 (2004) 39–45.
- [63] J.F. Bunnett, in: C.F. Bernasconi (Ed.), *Investigation of Rates and Mechanisms of Reaction Part 1*, 4th ed., Wiley Interscience, New York, 1986, p. 285.
- [64] R.K. Singh, G.P. Kothiyal, A. Srinivisan, Influence of iron ions on the magnetic properties of CaO-SiO<sub>2</sub>-P<sub>2</sub>O<sub>5</sub>-Fe<sub>2</sub>O<sub>3</sub> glass-ceramic, *Solid State Commun.* 146 (2008) 5–29.
- [65] M. Noorjahan, V.D. Kumari, M. Subrahmanyam, L. Panda, Immobilized Fe(III)-HY: an efficient and stable photo-Fenton catalyst, *Appl. Catal. B: Environ.* 57 (2005) 291–298.
- [66] N. Panda, H. Sahoo, S. Mohapatra, Decolorization of methyl orange using Fenton-like mesoporous Fe<sub>2</sub>O<sub>3</sub>-SiO<sub>2</sub> composite, *J. Hazard. Mater.* 185 (2011) 359–365.
- [67] B. Neppolian, H.C. Choi, S. Sakthivel, B. Arabindoo, V. Murugesan, Solar light induced and TiO<sub>2</sub> assisted degradation of textile dye reactive blue 4, *Chemosphere* 46 (2002) 1173–1181.
- [68] S. Sakthivel, B. Neppolian, M.V. Shankar, B. Arabindoo, M. Palanichamy, V. Murugesan, Solar photocatalytic degradation of azo dye: comparison of photocatalytic efficiency of ZnO and TiO<sub>2</sub>, *Sol. Energy Mater. Sol. Cells* 77 (2003) 65–82.
- [69] I. Arslan, A.I. Balcioglu, D.W. Bahnemann, Photochemical treatment of simulated dye house effluents by novel TiO<sub>2</sub> photocatalysts: experience with the thin film fixed bed (TFFB) and double skin sheet (DSS) reactor, *Water Sci. Technol.* 44 (2001) 171–178.
- [70] Y.C. Chen, H.M. Lee, M.H. Huang, S.H. Chen, J.M. Yan, M.S. Yang, A discharge reactor with water-gas mixing for methyl orange removal, *Int. J. Plasma Environ. Sci. Technol.* 2 (2008) 113–118.
- [71] L.G. Devi, S.G. Kumar, K.M. Reddy, C. Munikrishnappa, Photodegradation of methyl orange an azo dye by advanced Fenton process using zero valent metallic iron: influence of various reaction parameters and its degradation mechanism, *J. Hazard. Mater.* 164 (2009) 459–467.
- [72] J. Guo, D. Jiang, Y. Wu, P. Zhou, Y. Lan, Degradation of methyl orange by Zn(0) assisted with silica gel, *J. Hazard. Mater.* 194 (2011) 290–296.
- [73] C.C. Liu, Y.H. Hsieh, P.F. Lai, C.H. Li, C.L. Kao, Photodegradation treatment of azo dye wastewater by UV/TiO<sub>2</sub> process, *Dyes Pigments* 68 (2006) 191–195.